AIAA SciTech Forum
23-27 January 2023, National Harbor, MD & Online
AIAA SCITECH 2023 Forum

10.2514/6.2023-1773

Development of a Large-Scale Thermosyphon for Cooling the Fault Management System of a MW-Scale Electric Aircraft

Jeff Diebold[1], Brett Leitherer[2], Calin Tarau[3], Kuan-Lin Lee[4]
Advanced Cooling Technologies, Lancaster, PA, 17601, USA

Thermal management represents a significant challenge for electric aircraft due to the large quantity of low-grade waste heat that must be dissipated. To solve this challenge, a lightweight solid-state thermal management system for MW-scale hybrid electric aircraft is being developed. The system utilizes an acoustic heat pump to actively cool electronic components and elevate the temperature of the heat. The waste heat is then recycled by distributing it throughout the aircraft via a network of heat pipes and thermosyphons. By recycling the waste heat, the overall system efficiency can be improved. This paper will specifically focus on the design and testing of a thermosyphon network for distributing the waste heat generated by the DC fault management system of the aircraft. The thermosyphon will be capable of extracting 5kW of heat from the hot end of the acoustic heat pump and delivering this heat to various locations on the aircraft that can benefit from thermal energy.

I. Nomenclature

ACT = Advanced Cooling Technologies
DC = Direct Current
NCG = Non-Condensable Gas
VCHP = Variable-Conductance Heat Pipe

II. Introduction

Electric aircraft propulsion systems, for MW-scale aircraft, come in a variety of configurations and many of these configurations share the need to utilize DC circuit breakers to provide protection against electrical faults. For MW-scale electric aircraft, solid-state DC circuit breakers provide important benefits, including extremely fast response time, simple structure, and low mass.[1] The drawback to a solid-state circuit breaker is the high conduction losses compared to other breaker technology.[2] Approximately 5-10kW of low-grade waste heat is produced for each MW-scale circuit breaker in the system. These losses reduce the overall efficiency of the system and present a significant thermal management challenge due to relatively low temperature of the waste heat. By elevating the temperature of the circuit breaker waste heat and then recycling the waste heat on board the aircraft, it is possible to maintain a high system efficiency while taking advantage of the benefits of solid-state circuit breakers.[1,3]

A solid-state (no moving parts) thermal management system for electric aircraft that elevates the temperature of low-grade waste heat via a thermoacoustic heat pump and then distributes that waste heat to various end users on board the aircraft via a network of passive heat pipes is being developed by NASA Glenn Research Center and Advanced Cooling Technologies (ACT).[1,4,5,6] In this system, a thermoacoustic heat pump is used to actively cool the solid-state DC breaker, and a heat pipe network[5,6] is used to extract the waste heat from the hot end of the heat pump and passively distribute the thermal energy throughout the aircraft. This paper will discuss the development of a large-scale thermosyphon, a passive two-phase heat transfer device designed by ACT, that collects heat from the hot end of the thermoacoustic heat pump. The waste heat is then transported to the wings where it can be used for anti-icing or

[1] R&D Engineer II, Research and Development
[2] R&D Engineer I, Research and Development
[3] Principal Engineer, Research and Development
[4] Lead Engineer, Research and Development

rejected into the atmosphere. In addition, by utilizing variable conductance heat pipe technology, the network can also deliver waste heat to various end users when required.

This work is being conducted under a Phase III SBIR program, and this paper summarizes work performed during Year 2 of the program. Work performed during Year 1 was summarized in Diebold et al.[5,6]

III. Thermosyphon Based Thermal Management System

A. Overview of Thermal Management System

A conceptual layout of the thermal management system, developed by Dyson et al.,[1] is shown in Figure 1a. Acoustic heat pumps are used to actively cool various electronic components, such as the DC breaker. Networks of embedded heat pipes or thermosyphons are then used to passively transport the heat from the hot end of the heat pump to various locations on the aircraft. Figure 1b illustrates the potential layout of a multi-branched thermosyphon that passively transports heat, at elevated temperatures, from the thermoacoustic heat pump to the wings for icing protection and to an arbitrary end user that may require thermal energy such as warming cabin air. The multi-branched thermosyphon collects heat at a single evaporator but delivers the heat to multiple condensers.

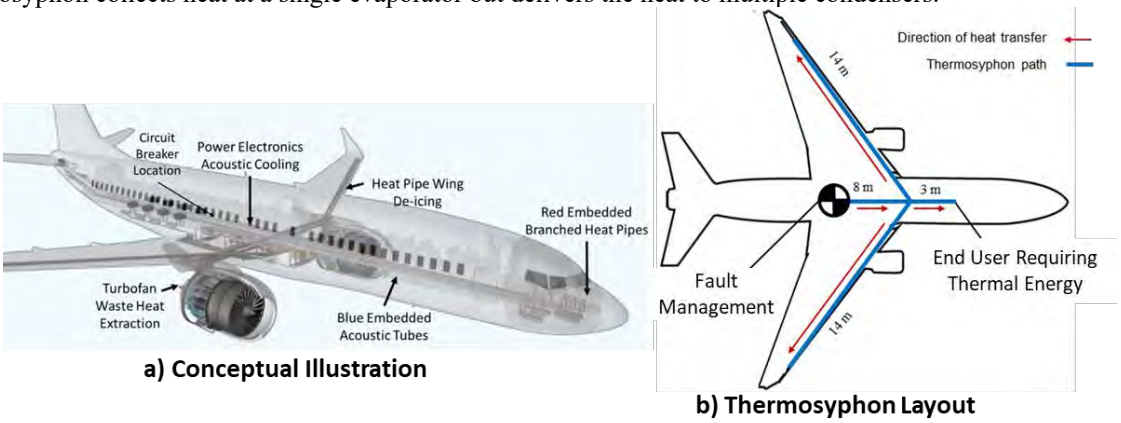

Figure 1. a) Conceptual illustration of the electric aircraft thermal management system[1], b) potential layout of multi-branched thermosyphon.

The DC breaker designed generates a total of 5kW of waste heat and will be cooled by three separate acoustic heat pumps each extracting approximately 1.6kW at the cold end of the pump. The hot end of each acoustic heat pump will then reject 5kW at approximately 100°C. The diameter of the acoustic heat pump tube was 4.0 in. and the length of the heat rejection region was 4.0 in. In total, the thermosyphon network will be required to remove 15kW from the ends of the separate acoustic heat pumps. This paper will focus on the design and testing of a single thermosyphon for carrying 5kW from a single acoustic heat pump.

B. Thermosyphon Design

A thermosyphon, also known as a gravity-aided heat pipe, is a passive two-phase heat transfer device. Within the evaporator, working fluid absorbs heat through the latent heat of vaporization. Vapor then flows to the condenser and releases the heat via condensation. By placing the evaporator below the condenser, the liquid can passively return to the evaporator due to gravity. By taking advantage of gravity, thermosyphons can transport large amounts of heat over long distances with minimal temperature drop, no moving parts, and no electrical power.

After finalizing the thermal requirements for the thermosyphon, ACT conducted a series of trade studies to determine the optimal working fluid and envelope material. When designing a heat pipe or thermosyphon, critical design parameters are the working fluid, envelope material, operating temperature, and the diameter of the pipe. The maximum power carried by a thermosyphon is typically restricted by the flooding limit,[7] which occurs at high powers when the vapor flowing from evaporator to condenser interferes with the falling liquid returning to the evaporator. Shear force between the counter flowing streams prevents the liquid from falling resulting in evaporator dry out. Unlike a typical capillary pumped heat pipe, the maximum power carried by the thermosyphon is not affected by the length. The flooding limit is primarily affected by the working fluid, operating temperature, pipe diameter, and angle relative to gravity.[7]

A trade study was conducted to compare different working fluids and envelope material combinations for this application. Table 1 compares thermosyphon designs for four envelope and working fluid combinations sized to carry 6.7kW at the flooding limit. This provides margin for the required 5kW. The working fluids considered are commonly

used in heat pipes around 100°C. Most potential working fluids in heat pipes are compatible with more than one envelope material. For this trade study, the considered envelope material contained the lowest density of the potential options compatible with the given working fluid. For example, water is commonly used with copper or nickel envelopes both of which have significantly higher density than titanium.

Of the fluids considered, it is well known that water is the best performer. As seen in Table 1, water requires the smallest diameter to achieve the power requirement. The required diameter is independent of the envelope material. To fully assess the working fluid and envelope combinations the mass per unit length (kg/m) and the specific power multiplied by length (W-m/kg) are the most relevant metrics. The specific power multiplied by length is used because the final length of the full-scale thermosyphon is unknown. By dividing this metric by a given length, the specific power of a design can be determined. These metrics show that water-titanium is the best combination, it requires the smallest diameter and has the lowest mass.

Table 1. Results of thermosyphon trade study. Thermosyphons sized based on flooding limit of 6,670W at 100°C to provide margin for the 5,000W design criteria. Specific power was calculated based on 5000W. An angle of 5° relative to the horizontal was assumed.

Parameter	Toluene	Methanol	Acetone	Water
Envelope Material	Aluminum	316 SS	Aluminum	Titanium
Min Fluid Operating Temp	-50	-60	-50	20
Max Fluid Operating Temp	280	100	100-120	280
Outer Pipe Diameter (in)	3	1.75	2.5	1.25
Available Wall Thickness (in)	0.035	0.028	0.035	0.02
Mass Per Unit Length (kg/m)	0.57	0.818	0.474	0.225
Specific Power * Length (W-m/kg)	8,804	6,116	10,590	22,285

IV. Water-Titanium Thermosyphon Prototype Design and Fabrication

Based on the trade studies discussed above, ACT decided to design and build a reduced-scale but full power (5kW) water-titanium thermosyphon prototype with geometry relevant to an aircraft. Figure 2 shows a complete CAD model of the full reduced-scale water-titanium thermosyphon prototype. The thermosyphon was supported by an aluminum frame which was mounted on rounded supports capable of rotating about two-axes to simulate aircraft pitch and roll. The prototype was designed for full-scale power of 5kW at the operating temperature of 100°C, but the overall dimensions of the system are reduced compared to what would be used in a full-scale aircraft. The thermosyphon system contained a single evaporator to extract heat from an acoustic heat pump and three separate condensers, two representing the wings and a single end user located towards the nose of the aircraft, for applications such as warming cabin air. The complete prototype was approximately 5m in length but the total thermosyphon length, including the wings, was approximately 9m. Each branch of the thermosyphon was at angle of 5° relative to the horizontal.

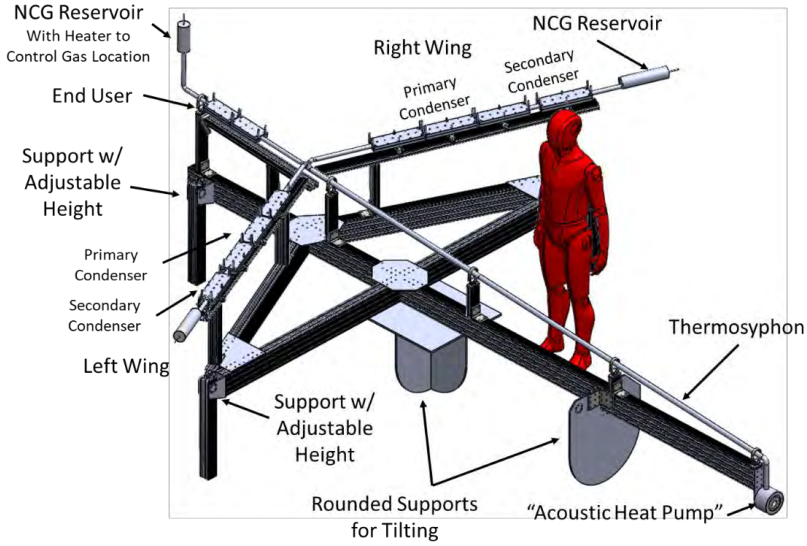

Figure 2. CAD model of reduced-scale water-titanium thermosyphon prototype on the aluminum frame. The frame was designed to tilt to simulate aircraft pitch and roll.

It was assumed that the wings could receive an arbitrary amount of heat and that it may be desired to block heat transfer to the central end user. This capability was accomplished with variable conductance heat pipe technology (VCHP). Each condenser had a reservoir of non-condensable gas (NCG). When the thermosyphon operates, the flowing vapor pushes the NCG towards the condensers and into the reservoirs at the end of each branch. The reservoir for the central end user could be heated to

expand the NCG and block vapor from reaching the central end user condenser. Reservoirs at the ends of each wing were used for storing excess NCG during operation. In previous work, ACT successfully demonstrated the proper sizing of NCG reservoirs in a multi-branched heat pipe for passively controlling the distribution of NCG in each branch.[5,6]

An image of the completed water-titanium thermosyphon is shown in Figure 3a, and Figure 3b shows the insulated prototype in the tilted position during an experiment. Figure 3a also shows the annular evaporator that would wrap around the hot end of a thermoacoustic heat pump. The inner surface of the annular evaporator contained a porous wick to help distribute working fluid on the heated surface. A thermoacoustic heat pump was not available for testing so a custom 5kW heater was designed, see Figure 3a. The heater was a stainless-steel cylinder with 12 individual heater cartridges. It should be noted that this heater design results in significant thermal resistance due to the contact resistance between the stainless-steel heater and the titanium evaporator. Future evaporator designs will be intimately integrated with the thermoacoustic heat pump to eliminate this thermal resistance.

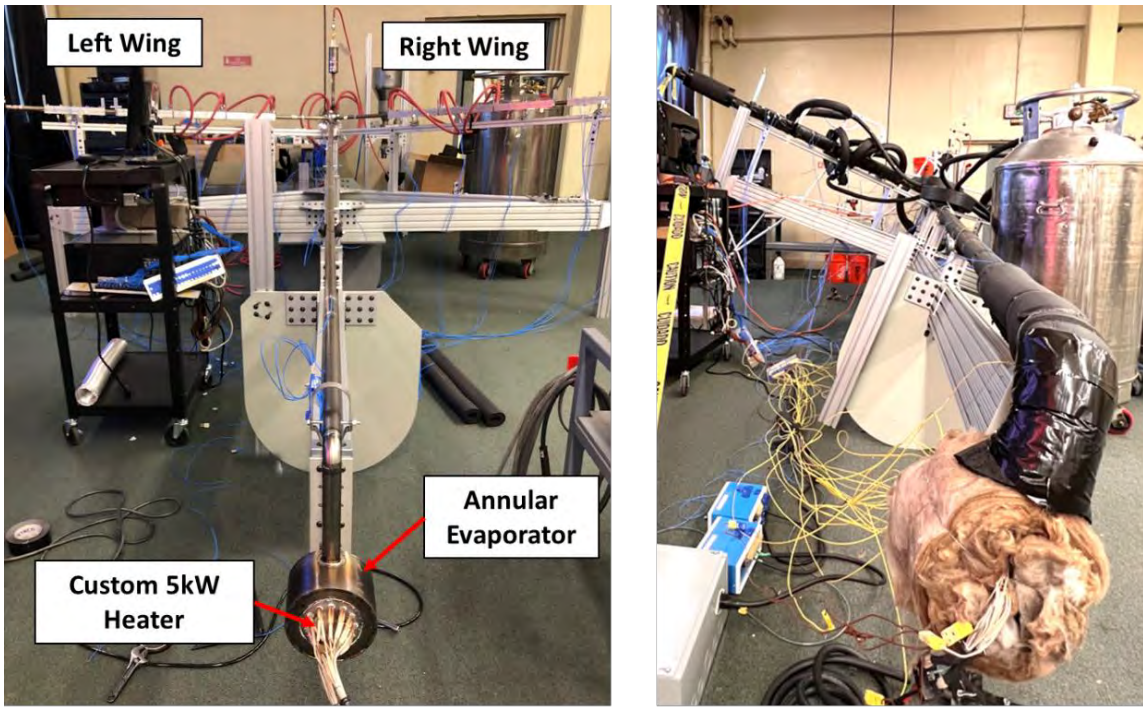

Figure 3. a) Image of the completed water-titanium thermosyphon. b) completed thermosyphon insulated and tilted 20° right wing down during an experiment.

V. Water-Titanium Thermosyphon Prototype Testing

Experimental testing of the reduced scale water-titanium thermosyphon prototype had several goals:

- Demonstrate the distribution of NCG during thermosyphon startup
- Demonstrate the ability to carry the target heat load of 5kW
- Demonstrate continued operation while the system is tilted (aircraft is banked)
- Demonstrate the ability to shutdown heat transfer to the central end user by heating the corresponding NCG reservoir

This section will highlight a few key experimental results.

A. Thermosyphon Startup

The first thermosyphon feature observed experimentally was startup behavior. Prior to applying power, when the system is at ambient temperature, most of the working fluid is in a liquid state in the evaporator. The rest of the

thermosyphon volume is occupied by NCG. As the vapor temperature rises, the corresponding increase in vapor pressure begins to compress the NCG towards the reservoirs of the three branches (two wings and one central end user). This is illustrated in Figure 4, which shows how vapor and NCG are distributed at some arbitrary vapor temperature that is below the design operating temperature. The thermosyphon's intended operating temperature was 100°C. The reservoirs were sized and the amount of NCG was selected so that the NCG/vapor front reached the points indicated in Figure 4 at the design operating temperature of 100°C. The wings had larger reservoir volumes allowing the NCG front to move further for a given change in vapor pressure compared to the NCG front in the central end user branch. As a result, the NCG front within the wings were able to move a longer distance for the same change in vapor pressure.

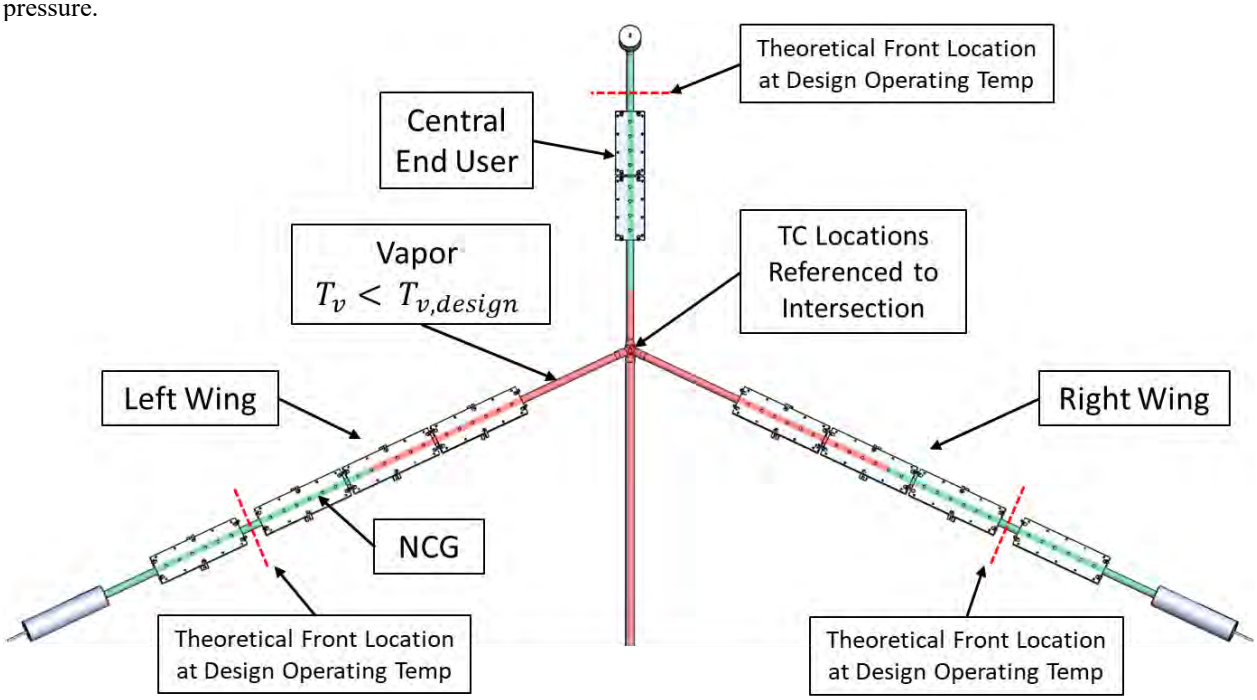

Figure 4. Illustration of startup process when the vapor temperature is below the design operating temperature. As the vapor temperature rises, the increasing vapor pressure compresses the NCG towards reservoirs of each branch. The predicted locations of the NCG front in each branch at the design operating temperature of 100°C are indicated by the red dashed line.

Figure 5 shows the temperature profiles along the wings and the central end user at several times during the startup process where a constant power of 2kW was applied at the evaporator. The first plot, Figure 5a, was an arbitrarily selected point in time shortly after the NCG front had passed the intersection of the three branches. The temperature measurement locations were referenced to the intersection as indicated above in Figure 4. As time progressed (Figure 5a to f) the front can clearly be seen moving along each branch as the vapor temperature increased towards 100°C. The plots show data covering a time span of approximately 25 minutes. The time to startup was a result of the power being applied at the evaporator and the significant thermal mass of the chiller blocks along the condensers of the three branches. Throughout the entire startup process the left and right wings had nearly identical temperature distributions as intended. On Figure 5f the theoretically calculated locations of the NCG fronts in each branch are indicated. The predicted front locations match the temperature distributions very well. The theoretical calculations assumed a "flat" front that is discontinuous between vapor and NCG. In reality, this front was diffused as vapor and NCG mix. In addition to this mixing, the front was further obscured by conduction through the envelope of the thermosyphon. Despite the limitations of the theory, the results of Figure 5f indicate that the reservoir sizing and NCG charging calculations were very accurate.

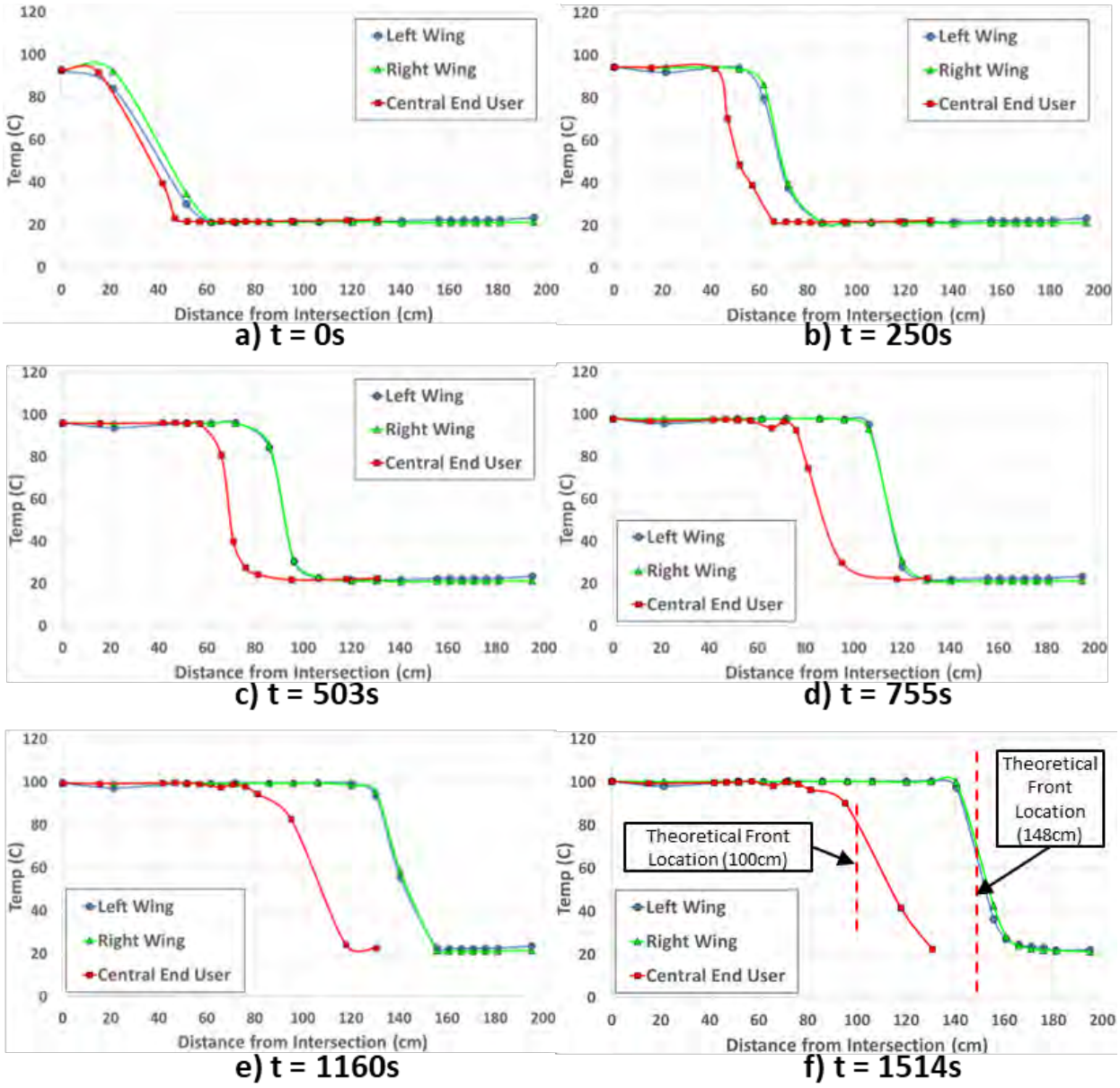

Figure 5. Temperature distributions along the wing and central end user branches of the thermosyphon during startup. 2kW were applied to the evaporator. TC locations are referenced to the intersection of the three branches, see Figure 4. The first graph t = 0, is an arbitrary reference point selected shortly after the front had reached the intersection of the three branches.

B. Thermal Resistance and Maximum Power

A key experimental finding was that the thermal resistance within the evaporator was a function of the volume of working fluid charged to the system. Evaporator thermal resistance was determined by measuring the temperature of a heater cartridge while maintaining the vapor temperature at the target 100°C. Figure 6 shows the maximum heater temperature (thermocouple on the heater cartridge) when 2kW was applied to the heater, as a function of the liquid charge volume. The total volume of the evaporator was 845cm^3.

Increasing the charge from 208cm^3 to 358cm^3 decreased the maximum temperature on the heater from 431°C to 278°C. A further addition of working fluid to 408cm^3 did not affect the maximum temperature. The total thermal resistance between the heater and the vapor for the minimum and maximum charge tested are indicated on Figure 6. The increase in working fluid reduced the thermal resistance by 46%.

It is important to note that the thermal resistance in this prototype is very high due to the use of the custom stainless-steel heater inserted into the titanium annular evaporator. Future prototypes will demonstrate an evaporator design integrated with the thermoacoustic heat pump to significantly reduce thermal resistance.

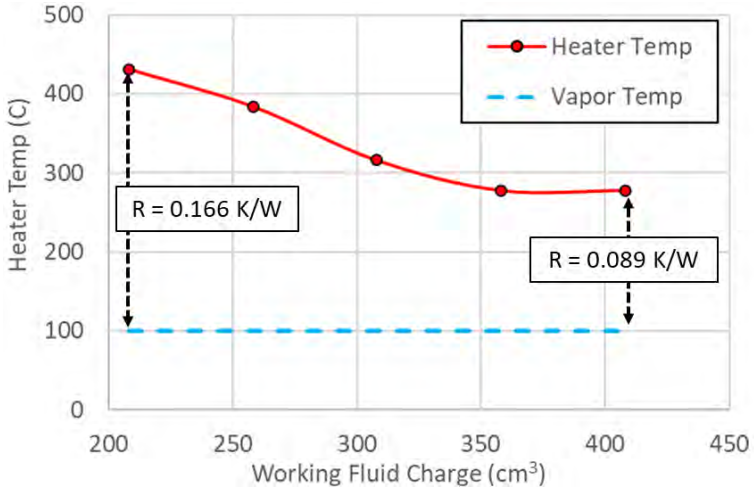

Figure 6. Maximum heater cartridge temperature for 2 kW applied to the evaporator and a vapor temperature of 100°C as a function of the working fluid charge.

After observing a significant reduction in thermal resistance, resulting from the increased amount of working fluid, the heater was turned up to maximum power. Figure 7 shows the heater temperature, adiabatic (vapor) temperature, and applied power vs. time during the experiment at the higher working fluid charge of 408cm^3. The vapor temperature was maintained at a constant 100°C by adjusting cooling as power was increased. During the experiment a maximum of 4.2kW was reached. At this point the heater had reached its maximum output. There was no indication that the thermosyphon had reached a limit. It is expected that with relatively minor alterations to the electronics controlling the heaters it should be possible to reach 5kW. This will be demonstrated in future work.

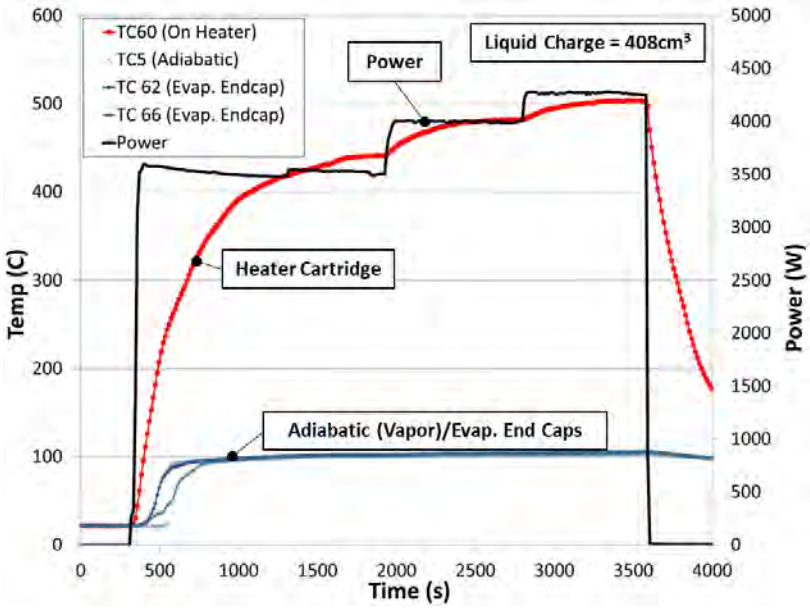

Figure 7. Effect of power on heater temperature for an increased charge of working fluid (408cm^3). Heater temperature is represented by a thermocouple welded directly to the surface of one of the heater cartridges. Vapor temperature was held constant as the power increased by adjusting the cooling applied at the condensers.

C. Operation During Tilt

The experimental setup shown above in Figure 2 was designed to tilt simulating the effect of aircraft banking during a turn. In the tilted configuration, shown in Figure 3b, one wing is down and any liquid condensing in this branch of the thermosyphon will pool at the end of the branch and cannot flow back to the evaporator. As a result, there is more mass leaving the evaporator as vapor than returning as liquid and the evaporator will eventually deplete the liquid inventory and dry out. In order to continue operating during a turn, the annular evaporator can utilize the excess liquid inventory to account for the decreased returning mass flow rate. A series of "Tilt until dry out" experiments were conducted by tilting the prototype, right wing 20° down, and monitoring the time taken to reach dry out.

"Tilt until dry out" experiments demonstrated that increasing the working fluid inventory significantly increased the time to maintain a steady temperature despite the reduced liquid return. Figure 8 compiles the data for the various experiments to show the time after tilting for the heater temperature to rise 5°C while maintaining constant power and cooling. This metric is an arbitrary but conservative measure for comparing the different experiments. Increasing the fluid charge from 208cm^3 to 408cm^3 increased the time before heater temperature rise from 121s to 564s (an increase by a factor of 4.7). In future designs ACT plans to design the evaporator to hold more liquid to increase the excess inventory and increase the time until dry out.

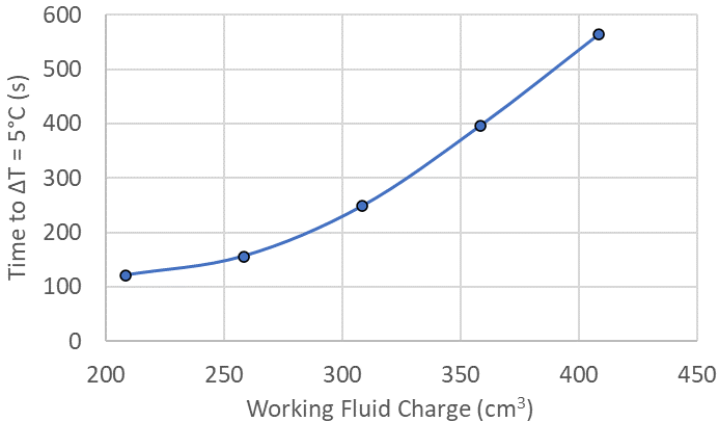

Figure 8. The time after tilt initiation for the cartridge heater temperature to increase by 5°C as a function of the working fluid charge in the system.

The presence of NCG reservoirs on the wings provides an additional benefit of extending the time until dry out. Recall that during a tilt, vapor will condense in the lower wing, but the liquid will pool at the end of the branch rather than return to the evaporator. This liquid will pool within the NCG reservoir at the end of the branch and displace the NCG into the condenser of the wing blocking vapor from this region. As a result, the area available for heat transfer within the lower wing will be reduced and the rate at which liquid is trapped within this wing will also decrease. Instead, the vapor will flow into the other wing that is still functioning as a thermosyphon. Figure 9 compares the temperature distributions along the left and right wing just prior to initiating a tilt and 10 minutes after tilting the right wing 20° down. Prior to tilting, the wing temperature distributions were identical, and each condenser was fully open. Ten minutes after tilting, the temperature distribution of the right wing changed dramatically. Liquid pooling in the condenser displaced the NCG front, blocking more of the right-wing condenser from seeing vapor and reducing the rate at which liquid was trapped in the right-wing reservoir.

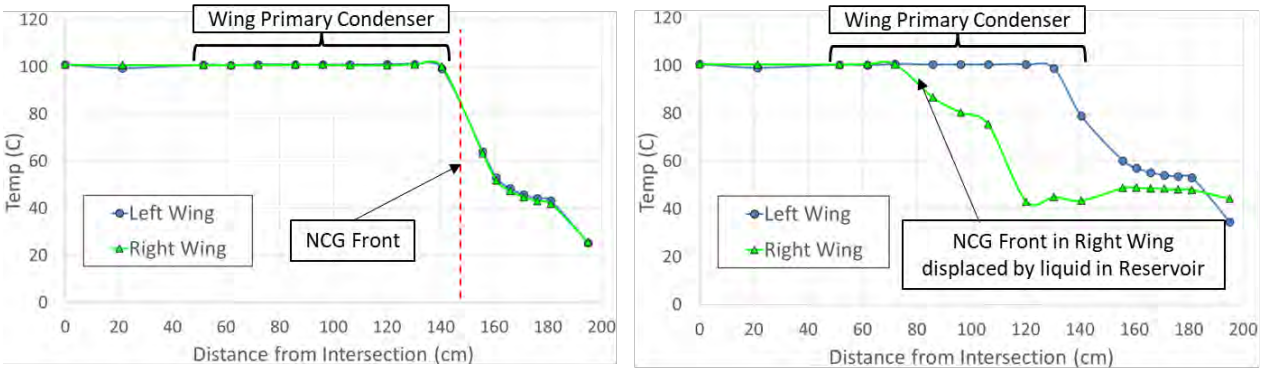

a) Before Tilt **b) 10 min of Tilt**

Figure 9. Temperature distributions along the left and right wing during a long tilt, 20° right wing down. Power = 2kW. Working fluid charge = 408cm^3. TCs corresponding to the wing's primary condenser are indicated.

D. VCHP Control of Central End User

By including NCG reservoirs on each branch of the thermosyphon it was possible to shut down heat transfer to the central end user by heating the corresponding NCG reservoir. Heating the central reservoir caused the NCG to expand into the central condenser preventing vapor from reaching this area. The NCG fronts in the wings were free to expand further along the wings compensating for the decrease in heat transfer area in the central thermosyphon branch. This feature provides a means of thermal control without the use of moving parts.

Figure 10a shows the heater temperature, vapor temperature, central reservoir temperature and the temperatures at the beginning and end of the central condenser during a VCHP control test with a constant 2kW applied to the evaporator. Figure 10b highlights the geometry and distribution of vapor and NCG during this experiment. At

approximately 7300s, the heater on the central reservoir was turned on. As the reservoir temperature increased, the temperature at the front end (towards the aircraft nose) of the central end user condenser began to decrease as the NCG/vapor boundary moved into the condenser, see Figure 10b. By approximately 9000s, the temperature at the back end (away from the aircraft nose/close to the evaporator) of the central end user condenser began to decrease as the NCG covered the entire central condenser. The reservoir temperature was then maintained at a constant value for approximately 1000s at which point the reservoir was rapidly cooled and the system returned to its original state. During this entire period, there were negligible changes in the vapor and heater temperature. Note that the time taken to heat the reservoir and shut down the central condenser was arbitrary, as it was controlled by how much power was applied to the reservoir.

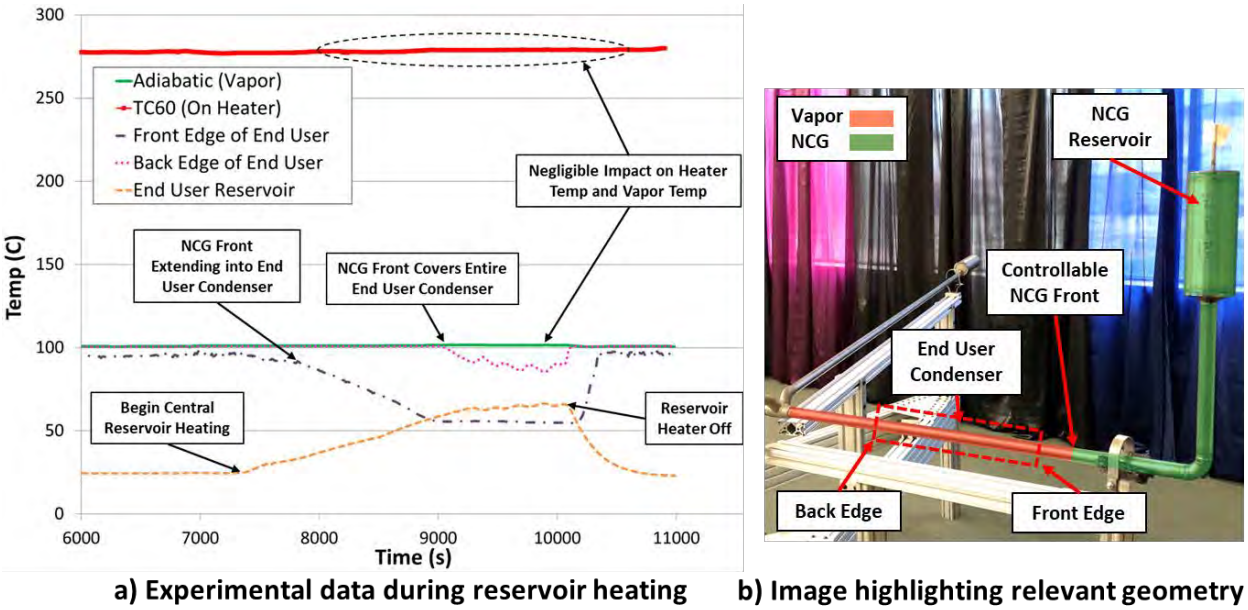

a) Experimental data during reservoir heating b) Image highlighting relevant geometry

Figure 10. a) Temperatures at various points on the thermosyphon during a VCHP control test. At approximately 7300s, the heater on the central NCG reservoir was turned on. Power = 2kW. Working fluid charge = 408cm^3, b) Image of the prototype highlighting the relevant geometry and location of vapor and NCG during this experiment.

The change in temperature distribution along the central end user branch while the reservoir heats up can be clearly seen in Figure 11. In Figure 11a, the central reservoir was still at the ambient temperature and the NCG front within the central branch was located just beyond the edge of the central end user condenser. In Figure 11b, the central reservoir temperature had increased to 40°C and the NCG front was pushed approximately halfway through the central end user condenser. By the time the reservoir had reached approximately 60°C (Figure 11d) the NCG front had moved beyond the central end user condenser fully blocking vapor from this region. Note that the front had not yet reached the intersection of the three branches ensuring the NCG distribution between the branches remained unchanged. There was a slight increase in the temperatures along the outer portions of the wing.

This method of thermal control, heating/cooling a reservoir of NCG, is only dependent on temperature of the gas and the vapor. The temperature of the reservoir will drive the expansion or contraction of the gas within the thermosyphon condenser independent of how much power the thermosyphon is transporting. A relatively small amount of power delivered to the NCG reservoirs can be used to control an arbitrary amount of power transferred through the thermosyphon system. Maintaining the reservoir at a constant elevated temperature to keep the central condenser closed only requires enough power to overcome heat leaks form the reservoir.

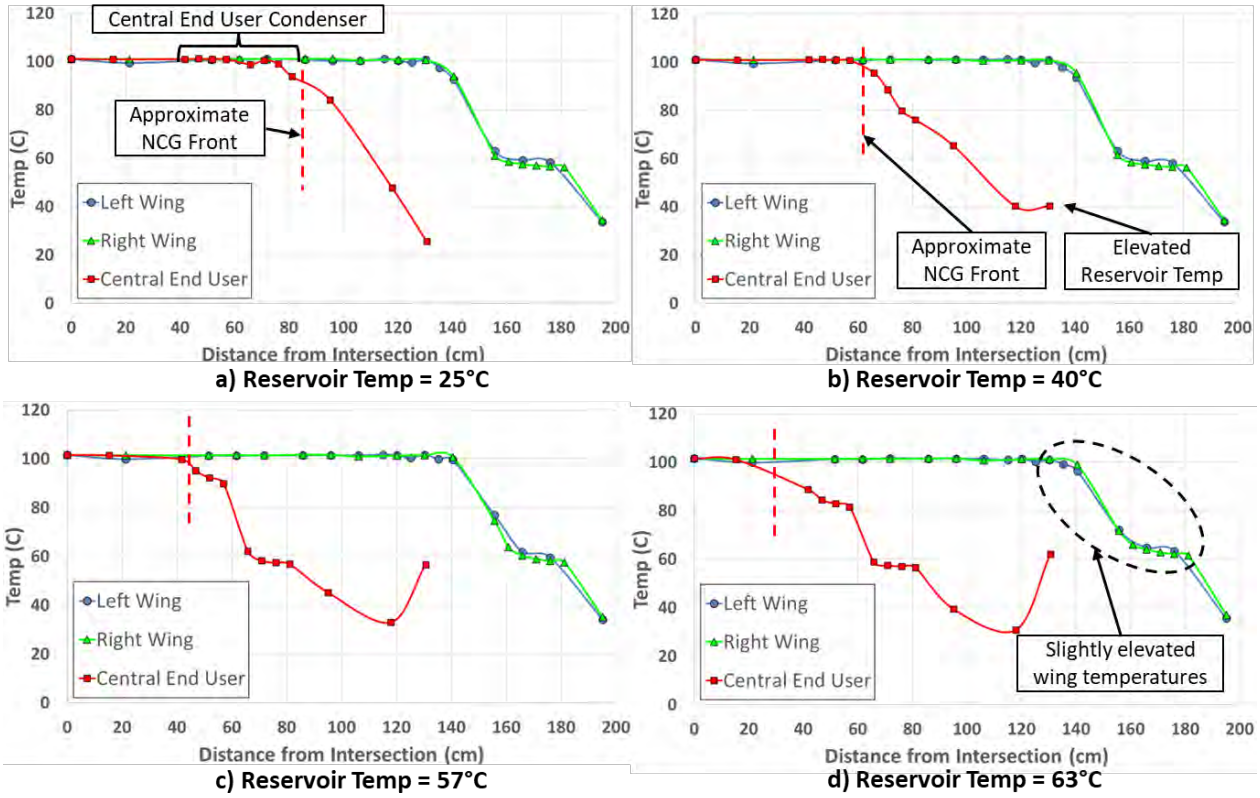

Figure 11. Temperature distributions along the wings and the central branch of the thermosyphon during a VCHP control test. The heater on the central NCG reservoir was used to increase the temperature of the NCG in order to block vapor from reaching the central end user. The approximate location of the NCG front in the central end user branch is indicated in each plot. Power = 2kW. Working fluid charge = 408cm^3.

VI. Conclusion

The following is a list of key results from ACT's work developing the high-power reduced-scale thermosyphon prototype for electric aircraft fault management cooling:

- Thermosyphon trade studies indicated a water-titanium thermosyphon was the best option from a mass and volume perspective.
- ACT designed a reduced-scale but full-power water-titanium thermosyphon prototype. The prototype had several key features:
  - An annular evaporator that could interface with the thermoacoustic heat pump.
  - Three separate branches representing different condensers. One for each wing and a central end user.
  - Each branch of the thermosyphon had a dedicated reservoir for NCG.
  - The central end user reservoir could be independently heated, in order to shutdown heat transfer to the end user.
  - The entire experimental setup was designed to tilt in order to simulate the aircraft banking during a turn.
- **A maximum power of 4.2kW was reached.** This limit was imposed by the electronics powering the heater and not the evaporator or the thermosyphon. It is expected that with alterations to the electronics 5kW could easily be achieved.
- **The ability of the thermosyphon to operate at a steady state during a turn (one wing down and not returning liquid) was successfully demonstrated.** Increasing the amount of excess liquid in the evaporator significantly extended the amount of time before local dry out began occurring throughout the evaporator.

- **Heating the central NCG reservoir in order to block heat transfer to the central end user was successfully demonstrated.** During this period no change in temperature was observed at the evaporator or heater. The heat transfer to various end users can be successfully controlled without disrupting the cooling of the electronics.

The work discussed above was performed during Year 2 of a Phase III SBIR program. Year 3 of the program will include the following tasks:

- ACT and NASA Glenn will design, fabricate, and test a complete system demonstration, including thermoacoustic heat pump, a pulsating heat pipe-based heat exchanger for cooling electronics and the water titanium thermosyphon demonstrated in this paper.
- ACT will design and fabricate a new thermosyphon evaporator that is intimately integrated with the thermoacoustic heat pump in order to minimize thermal resistance.
- ACT will investigate freeze tolerant designs for the water-titanium thermosyphon.

Acknowledgments

This project is funded by NASA Glenn Research Center under a SBIR Phase III program (Contract 80NSSC21C0601). The technical monitor is Rodger Dyson. The authors would like to thank Jonathan Murray, Larry Waltman and Philp Texter their work fabricating the water-titanium thermosyphon prototype.

References

[1] R.W. Dyson, L. Rodriguez, M.E. Roth and P. Raitano, "Solid-State Exergy Optimized Electric Aircraft Thermal and Fault Management," *AIAA Propulsion and Energy Forum,* AIAA 2020-3576, Aug. 2020.
[2] Armstrong, M., "Architecture, Voltage and Components for a Turboelectric Distributed Propulsion Electric Grid," NASA/CR-2015-218440.
[3] R. Jansen, "NASA Electrified Propulsion Efforts," *NATO-AVT-RSY-323 Research Symposium*, 2019.
[4] Hendricks, T., Tarau, C. and Dyson, R., "Hybrid Electric Aircraft Thermal Management: Now, New Visions and Future Concepts and Formulations," 20th IEEE ITherm Conference, 2021.
[5] Diebold, J., Lee, K-L., Tarau, C. and Anderson, W., "Development of Solid-State Waste Heat Delivery System for Electric Aircraft," 20th IEEE ITherm Conference, 2021.
[6] Diebold, J., Tarau, C., Lee, K-L, Anderson, W. and Dyson, R.W., "Electric Aircraft Thermal Management Using a Two-Phase Heat Transport System with Solid State Thermal Switching Capability," *AIAA Propulsion and Energy Forum 2021*, AIAA 2021-3334, Aug. 2021.
[7] A. Faghri, Heat Pipe Science and Technology, CRC Press, pp. 387-397, 1995, CRC Press, 1995, pp. 387-397.